Crystal structures of human pancreatic α-amylase in complex with carbohydrate and proteinaceous inhibitors

Virginie NAHOUM*, Geneviève ROUX†, Véronique ANTON‡, Pierre ROUGÉ‡, Antoine PUIGSERVER†, Hilmar BISCHOFF§, Bernard HENRISSAT* and Françoise PAYAN*[1]

*Architecture et Fonction des Macromolécules Biologiques, CNRS-IFR1, 31 Chemin Joseph Aiguier, 13402 Marseille, France, †Laboratoire de Biochimie et Biologie de la Nutrition, URA-CNRS 1820, Faculté des Sciences et Techniques de St Jérôme, Université Aix-Marseille, France, ‡Institut de Pharmacologie et de Biologie Structurale, UPR 9062, 205 route de Narbonne, 31077 Toulouse Cedex, France, and §Bayer AG, Institute for Cardiovascular and Arteriosclerosis Research, D-42096 Wuppertal, Germany

Crystal structures of human pancreatic α-amylase (HPA) in complex with naturally occurring inhibitors have been solved. The tetrasaccharide acarbose and a pseudo-pentasaccharide of the trestatin family produced identical continuous electron densities corresponding to a pentasaccharide species, spanning the −3 to +2 subsites of the enzyme, presumably resulting from transglycosylation. Binding of the acarviosine core linked to a glucose residue at subsites −1 to +2 appears to be a critical part of the interaction process between α-amylases and trestatin-derived inhibitors. Two crystal forms, obtained at different values of pH, for the complex of HPA with the protein inhibitor from *Phaseolus vulgaris* (α-amylase inhibitor) have been solved. The flexible loop typical of the mammalian α-amylases was shown to exist in two different conformations, suggesting that loop closure is pH-sensitive. Structural information is provided for the important inhibitor residue, Arg-74, which has not been observed previously in structural analyses.

Key words: acarbose, α-amylase inhibitor, transglycosylation, X-ray crystallography.

INTRODUCTION

α-Amylases (1,4-α-D-glucan glucanohydrolase, EC 3.2.1.1) catalyse the hydrolysis of α-1,4 glycosidic linkages in starch and related polysaccharides. α-Amylases belong to family 13 in the classification of glycoside hydrolases [1]. Family 13 is the most diverse of all glycoside hydrolase families, with many other enzyme activities, including α-dextrin endo-1,6-α-glucosidase (EC 3.2.1.41), cyclomaltodextrin glucanotransferase (CGTase; EC 2.4.1.19), cyclomaltodextrinase (EC 3.2.1.54), α,α-phosphotrehalase (EC 3.2.1.93), oligo-1,6-glucosidase (EC 3.2.1.10), glucan 1,4-α-maltohydrolase (EC 3.2.1.133), neopullulanase (EC 3.2.1.135), α-glucosidase (EC 3.2.1.20), glucan 1,4-α-maltotetraohydrolase (EC 3.2.1.60), isoamylase (EC 3.2.1.68), glucan 1,6-α-glucosidase (EC 3.2.1.70), glucan 1,4-α-maltohexaosidase (EC 3.2.1.98), 1,4-α-glucan branching enzyme (EC 2.4.1.18), trehalose synthase (EC 5.4.99.16), 4-α-glucanotransferase (EC 2.4.1.25), maltopentaose-forming α-amylase (EC number not yet assigned) and amylosucrase (EC 2.4.1.4). The glycoside hydrolase sequence families are now available at the web site http://afmb.cnrs-mrs.fr/~pedro/CAZY/db.html [2]. Although sharing the same global fold and catalytic machinery, the members of family 13 are therefore able to perform various reactions, such as hydrolysis, transglycosylation, condensation and cyclization.

The known three-dimensional structures of family 13 enzymes all consist of a typical $(\beta/\alpha)_8$ barrel, corresponding to the catalytic domain, accompanied by a varying number of additional surrounding domains. In all the known structures of α-amylases, two domains are invariably associated with the central $(\beta/\alpha)_8$ barrel. Despite the wealth of biochemical data available for this system, oligosaccharide complexes of human α-amylase have so far escaped structural characterization.

Human pancreatic α-amylase (HPA) is a 56 kDa protein consisting of 496 amino acids in a single polypeptide chain, folded into three domains [3]. The $(\beta/\alpha)_8$ barrel (domain A) contains a V-shaped depression similar to that described in the structure of pig pancreatic α-amylase (PPA) [4], which corresponds to the active site. A meandering loop that exists between the third β-strand and the third helix of the $(\beta/\alpha)_8$ barrel is called domain B. The C-terminal domain shows an eight-stranded, β-sheet structure. A chloride ion and a calcium ion are located in close proximity to the V-shaped depression. Recently, the crucial role of residue Asp-197 as the catalytic nucleophile in HPA has been demonstrated by Withers and co-workers [5].

As part of a study of the mechanism of HPA, we report here a structural analysis of the interactions among HPA and various inhibitors, showing the network of hydrogen bonds formed by the residues of the active site, and also by those from areas distant from the active site and yet involved in the inhibition process.

MATERIALS AND METHODS

Purification and crystallization

HPA–acarbose and HPA–B4 complexes

Highly purified HPA was obtained as described previously [6]. Crystallization was achieved at room temperature in hanging drops containing 2 μl of enzyme solution (18 mg/ml) and 2 μl from the reservoir containing 0.1 M Mes (pH 6.5) and 55% (v/v) 2-methyl-2,4-pentanediol. Pure species of acarbose and B4 (pseudo-pentasaccharide) compounds were from Bayer Pharma, Wuppertal, Germany. The soaking solutions were prepared by dissolving the carbohydrate inhibitors in the mother

Abbreviations used: α-AI, α-amylase inhibitor; CGTase, cyclomaltodextrin glucanotransferase; E/I, enzyme/inhibitor; HPA, human pancreatic α-amylase; MR, molecular replacement; PEG, poly(ethylene glycol); PPA, pig pancreatic α-amylase; V_m, volume of asymmetric unit/molecular mass.

[1] To whom correspondence should be addressed (e-mail fran@afmb.cnrs-mrs.fr).

Table 1 Data collection and refinement statistics

Data statistics for the last shell are given in parentheses. $R_{merge} = \Sigma_h \Sigma_i |I_{h,i} - \langle I_h \rangle| / \Sigma_h \Sigma_i |I_{h,i}|$. R_{cryst} is defined as $\Sigma |F_o - F_c| / \Sigma |F_o|$. R_{free} is calculated in the same way on a subset of reflections that are not used in the refinement, where F_o and F_c are the observed and calculated structure factors respectively. CC, correlation coefficient; r.m.s.d., root mean square deviation.

	Inhibitor–HPA complexes			
Parameter	α-AI–HPA1	α-AI–HPA2	Acarbose–HPA	B4–HPA
Space group	C2	C2	$P2_12_12_1$	$P2_12_12_1$
a (Å)	151.543	163.331	53.110	53.283
b (Å)	80.122	73.525	75.120	75.649
c (Å)	69.165	68.401	137.127	137.971
β (°)	93.954	91.177	90.000	90.000
V_m ($Å^3 \cdot Da^{-1}$)/Solvent content (%)	2.72/54.7	2.66/53.7	2.49/50.6	2.55/51.7
Resolution limit (Å)	15–2.9 (2.98–2.90)	15–2.4 (2.46–2.40)	25–3.2 (3.27–3.20)	10–2.52 (2.58–2.52)
No. of measurements	68749 (5121)	123579 (9226)	45084 (2130)	101299 (4402)
Unique reflections	18332 (1357)	31750 (2371)	10103 (445)	16829 (891)
% of data $> 1\sigma$	85.8 (63.9)	87.1 (69.0)	90.6 (85.2)	95.8 (86.5)
Completeness	99.3 (99.3)	99.7 (99.7)	91.8 (63.4)	95.8 (76.9)
Average multiplicity	3.2 (3.1)	3.9 (3.9)	4.5 (4.8)	6.0 (4.9)
R_{merge}	0.079 (0.419)	0.102 (0.474)	0.158 (0.286)	0.079 (0.214)
$I/\sigma(I)$	8.8 (1.7)	7.0 (1.6)	9.2 (5.3)	11.3 (5.8)
B value (Wilson plot) ($Å^2$)	56	33	30	36
MR (R_f/CC)	0.195/0 .872	0.264/0.775	0.242/0.809	0.242/0.816
Refinement range (Å)	15–2.9	15–2.4	11–3.2	10–2.52
No. of reflections ($F > 1\sigma_F$)	18332	31750	8957	16774
R_{cryst}/R_{free}	0.178/0.260	0.176/0.219	0.191/0.217	0.155/0.215
No. of protein atoms	5573	5529	3938	3938
No. of water molecules	51	127	105	240
No. of carbohydrate atoms	56	56	54	54
B factor	Group	Individual	Group	Individual
Main-chain/side-chain atoms ($Å^2$)	29.01/35.45	24.64/25.57	7.6/9.5	21.5/24.1
Water molecules ($Å^2$)	37.29	25.91	15.3	38.0
Carbohydrate atoms ($Å^2$)	53.0	59.7	13.3	49.2
R.m.s.d. bond lengths (Å)	0.010	0.011	0.015	0.010
R.m.s.d. angles (°)	1.445	1.426	1.902	1.392
Estimated coordinate error [30]	0.29	0.25	0.30	0.23

liquor at a concentration of 1 mM. The acarbose–HPA and B4–HPA complexes analysed in the present study were formed by soaking crystals of HPA for 6 h at room temperature.

HPA–α-amylase inhibitor (α-AI) complexes (designated α-AI–HPA1 and α-AI–HPA2)

The α-AI was purified from *Phaseolus vulgaris* cv. Tendergreen seed flour as described previously [7]. The freeze-dried α-AI was dissolved in 0.1 M sodium acetate, pH 5.7, containing 0.01 mM $CaCl_2$. Before crystallization, appropriate volumes of both proteins (each at 10 mg/ml) were mixed to generate a stoichiometric mixture, which was left at room temperature for 1 h. The initial crystallization trials were performed using the hanging-drop, vapour-diffusion method [8], with a poly(ethylene glycol) (PEG)/LiCl Hampton Research Grid Screen [9]. Single crystals suitable for X-ray analysis were obtained after 2 weeks at room temperature in hanging drops consisting of 2 μl of complex solution and 2 μl from the reservoir, containing 0.1 M Mes (pH 6.3 for the first, or α-AI–HPA1, complex, and pH 7.8 for the second, or α-AI–HPA2, complex), 5% (v/v) PEG 6K and 1 M LiCl.

Data collection and processing

Crystals were mounted and sealed in capillaries with a drop of mother liquor. Each data set was collected at room temperature from a single complex crystal and recorded on a Mar-Research plate scanner developed by Hendrix and Lentfer (Hamburg, Germany) with conventional CuKα radiation. Data frames were recorded while the crystal was oscillated through 1 ° steps. The diffraction data were processed with the DENZO and SCALEPACK software [10]. The data collection statistics are given in Table 1.

Molecular replacement (MR)

HPA–α-AI complexes

The MR calculations were performed at 4 Å (0.4 nm) resolution using the program suite AMoRe [11]. The search models used were the refined 2.1 Å resolution structure of HPA (enzyme; E) [3] and one monomer (inhibitor; I) of the 1.85-Å-resolution structure of the inhibitor bound to PPA [12]. Two rotation functions were calculated [11], one for E and one for I. They both showed unambiguously a single solution corresponding to the orientation of HPA and α-AI respectively. After each translation function, the previously determined positions and orientations were refined in the form of rigid bodies [13] [see Table 1 for R-factor (R_f) and correlation coefficient (CC)]. In both structures, the MR process yielded an E_2I_2 complex model consistent with efficient packing, and one EI complex per asymmetric unit, which is in good agreement with the Matthews' coefficient values (V_m; a measure of the volume of asymmetric unit/molecular mass) [14].

HPA–carbohydrate complexes

Both structures were solved by MR using the AMoRe program packages [11]. The structure of free HPA [3] was used as the model for searching. In both crystal structures a unique solution was obtained, yielding good parameter values (see Table 1) and a final result consistent with efficient packing and one complexed HPA molecule per asymmetric unit, in good agreement with the V_m values.

Refinements

Refinement procedures (see Table 1 for parameter values) were performed using the XPLOR slow-cooling protocol [15] and incorporation of a bulk-solvent correction [16], followed by manual rebuilding into electron-density maps, with σ_A/likelihood weighting [17]. The group isotropic B-factor refinement procedure for both main-chain and side-chain atoms and individual ligands was applied when necessary. The R_{free} behaviour was monitored [18]. Water molecules were added to the model provided that the electron density was present at a level of at least 3σ in the $(F_{obs}-F_{calc})\exp(i\alpha_{calc})$ maps. The molecules introduced were inspected visually for correct geometry of hydrogen bonding; most of the molecules introduced in structures analysed at 3 Å resolution were present in the initial models.

HPA–carbohydrate complexes

It should be stressed that, even with the starting phases, clear-cut continuous densities corresponding to the oligosaccharide ligands were observed in the binding clefts of both structures. The template of a glucose residue to be used in the refinement of the ligand structure was on the basis of crystallographic data on individual monosugars, whereas that required for the acarviosine moiety (cyclitol and amino-sugar units) was taken from our previous highly refined PPA–acarbose complex. No oligosaccharide atoms were included in the procedure until the refinement of the protein had reached convergence. The electron-density maps (with σ_A weighting) calculated before the incorporation of any sugar moiety were carefully examined. In order to identify the sugar units, difference maps were calculated, giving zero occupancy to the O-6 atoms.

The quality of the models was assessed using the PROCHECK program [19]. All the residues were located in generously allowed regions, except for a few HPA residues (as previously found in the free enzyme structure [3]) and residue Tyr-186 of the proteinaceous inhibitor α-AI (strongly hydrogen-bonded to the catalytic residue Asp-197). All structures include one Cl^- ion and one Ca^{2+} ion in the enzyme structure molecule. The structure-quality statistics are described in Table 1.

Coordinates for the structures described in this work will be deposited with the Brookhaven Protein Data Bank.

RESULTS AND DISCUSSION

Structure of HPA bound to trestatin inhibitors

Two members of the trestatin family of compounds were used in this study, the pseudo-tetrasaccharide acarbose and the pseudo-pentasaccharide called B4 (see Figure 1A).

Quality of the model and difference electron-density map

A summary of the data quality and completeness is given in Table 1. At the 1σ level in the final $(2F_{obs}-F_{calc})\exp(i\alpha_{calc})$ map, the model showed a well-defined electron density and, as observed in the free HPA structure [3], an excellent density was observed at the N-terminus corresponding to the pyrrolidone ring formed by the Gln-1 residue.

In the two complexed HPA structures, initial difference Fourier analysis showed clear continuous electron-density patterns corresponding to the oligosaccharide ligand present in the V-shaped depression. These initial difference electron-density maps (with σ_A weighting) were carefully examined prior to the incorporation of any sugar moiety. Despite the different initial inhibitor structures used in the study, the ligand present in the active site of the enzyme in both complexed structures was consistent with the same pentasaccharide species occupying subsites -3 to $+2$ of the active site (Figures 1A and 1B). The typical kink conformation of the ligand observed previously in other crystallographic studies of acarbose in interaction with α-amylases, and caused by a flip of ring surfaces between binding subsites -1 and $+1$, is conserved in the two complexes. The acarviosine unit was bound to subsites -1 and $+1$. The possibility of fitting the five-unit structure of the initial B4 molecule to the observed density in the HPA–B4-complex structure was checked and rejected. Consequently, it would appear that, as a general rule, a basic element of structure composed of the acarviosine unit and a glucose unit remain bound to the subsites -1, $+1$ and $+2$ of the α-amylases' active site. Moreover, the electron-density patch observed at subsite -2 unambiguously accommodates glucose units. Therefore the results suggest that, in the interaction process between trestatin-derived compounds and α-amylases, recognition of glucose, valienamine, 4-amino-4,6-dideoxy-α-D-glucose and glucose units at subsites -2, -1, $+1$ and $+2$ respectively is a predominant binding mode. The overall structure of the final ligand observed bound to the active site may be interpreted in terms of transglycosylation, as was suggested previously [20–23]. A possible transglycosylation scheme giving rise to the observed electron density is given in Figure 1(A). In the present study, the electron density (with five subsites occupied) observed in the structure of complex B4–HPA was not appropriately refined as a single B4 molecule (pseudo-pentasaccharide). This would be in keeping with occurrence of 'bi-reaction' events, during the interaction between trestatin-derived inhibitors and crystals of α-amylases, which probably give rise to the major bound product. Similar 'bi-reaction' events, such as transglycosylation and condensation, have also been proposed in a recent structural analysis of maltose and acarbose complexed with the maltogenic α-amylase from *Bacillus stearothermophilus* [24]. Our transglycosylation pattern appears to be in excellent agreement with this study.

The trestatin-derived inhibitors lying in the V-shaped depression make extensive hydrogen-bonding and hydrophobic contacts with the enzyme active-site residues (Figure 2A and Table 2). The role of Asp-197 as the catalytic nucleophile in the active site of human α-amylase has been demonstrated recently [5]. The present results show that the whole hydrogen-bonding network around this residue is highly conserved in both complexed HPA structures.

The only residue involved in the hydrogen-bonding network of HPA that is different from PPA is residue Thr-163 (replacing a valine in PPA). This residue, which is involved in the architecture of subsite -2, protrudes into the area surrounded by the trestatin-derived ligand bound to the active site, and is located in front of residues bound at subsites -2, -3 and $+1$.

The propyl group of Val-163 has been shown to protrude directly into the top of the α-cyclodextrin group bound to the active site of PPA [25]. A similar feature with a hydrophobic amino acid (Leu-600) exposed to solvent, involved in binding an α-cyclodextrin molecule by inserting its aliphatic side chain into

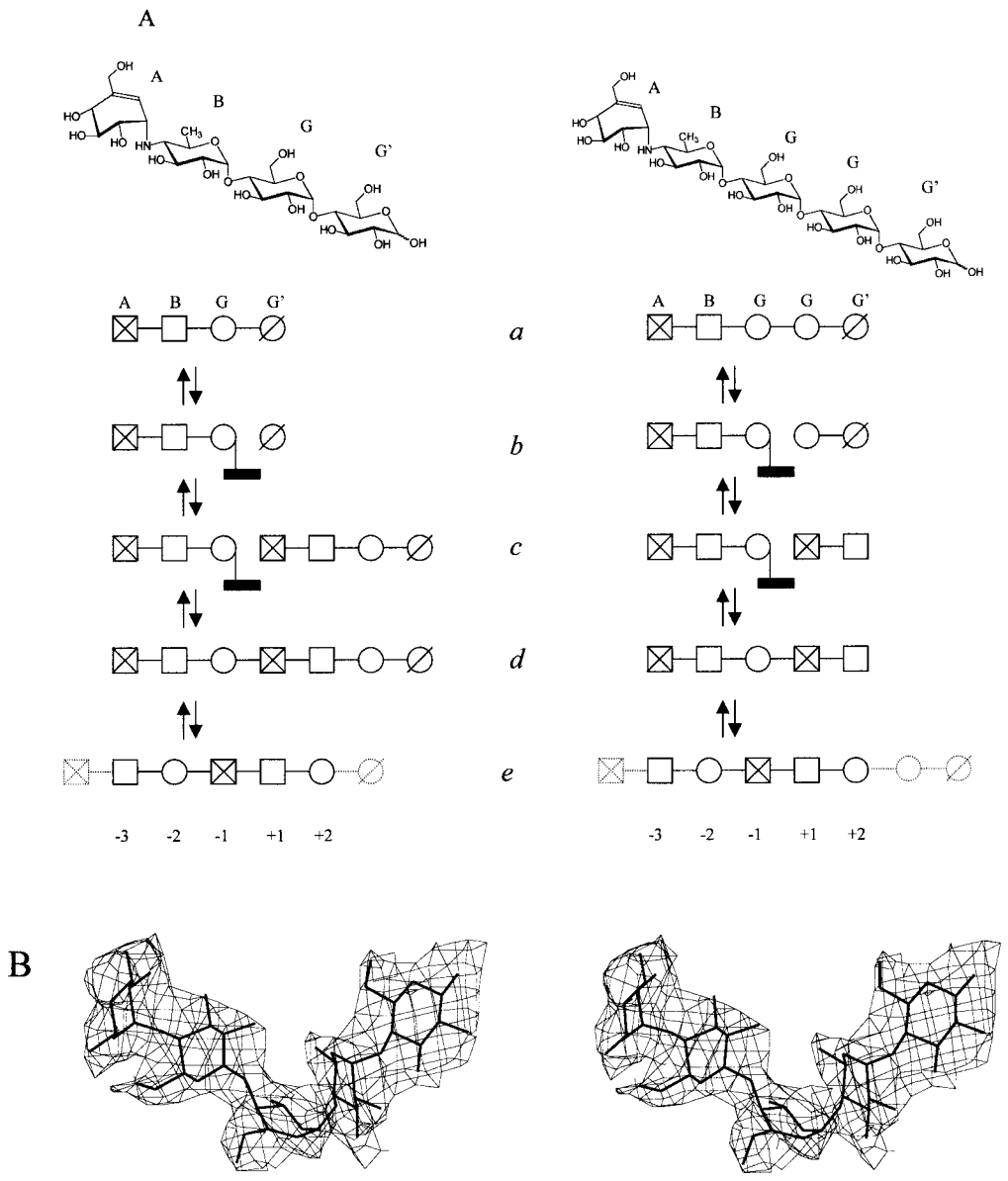

Figure 1 Trestatin-derived inhibitors

(**A**) Structures of acarbose (left) and B4 (right) compounds [31]. A = valienamine unit; B = 4-amino-4,6-dideoxy-α-D-glucose (AB is commonly referred to as the acarviosine moiety); G = α-D-glucose; G' = D-glucose. A scheme for the formation of the observed ligand from acarbose and from pentasaccharide B4 is proposed. The relevant enzyme subsites (nomenclature used according to Davies et al. [32], with cleavage taking place between subsites −1 and +1) are indicated. The reaction commences by binding of the ligands with the acarviosine moiety in the −3, −2 subsites (*a*); the reaction takes place via a covalent glycosyl enzyme intermediate (*b*), with release of glucose in the case of acarbose, and maltose in the case of pentasaccharide B4; (*c*) replacement of glucose/maltose by excess acarbose or pentasaccharide B4 permits transglycosylation (*d*). A shift of the transglycosylation product by one subsite can occur (*e*). Note that species *d* are hydrolysable, and therefore cannot accumulate; on the other hand, species *e* are not hydrolysable and can accumulate. The dotted lines indicate the parts which are not seen in the electron density, presumably because of disordering. (**B**) Stereoscopic view of the final (2 $F_{obs} - F_{calc}$)exp(iα_{calc}) electron density for the pentasaccharide ligand; the refined coordinates are shown.

the cyclodextrin ring, was observed in crystallographic studies of CGTase–substrate interactions [22]. It was suggested that this site is intended to bind cyclic or helical polysaccharides, such as cyclodextrins and amylose, and that mutation of this residue could reduce the binding of cyclic products. In the HPA structure, the presence of a threonine instead of a valine residue at position 163 might introduce some specificity in the interaction with amylose.

Conformational changes

When the native structure of HPA is compared with that in complex with acarbose and compound B4, a rotation of the loop formed by residues 303–312 towards the ligand is observed. In the free structure of HPA [3], this loop apparently assumes a conformation different from that in the free PPA structure [4] (Figure 2B). These different conformations were rather surprising, given the identical sequence of this 'flexible loop' in the pig and human enzymes.

The side chain of the catalytic residue Asp-300 shows the same orientation in both the free structure [3] and the present complexed structures of HPA. This is in contrast with pig α-amylase, which undergoes an induced conformational change of this residue upon substrate binding [20] (Figure 2B).

An additional area that undergoes significant conformational changes is the loop extending from residues 237–240, which

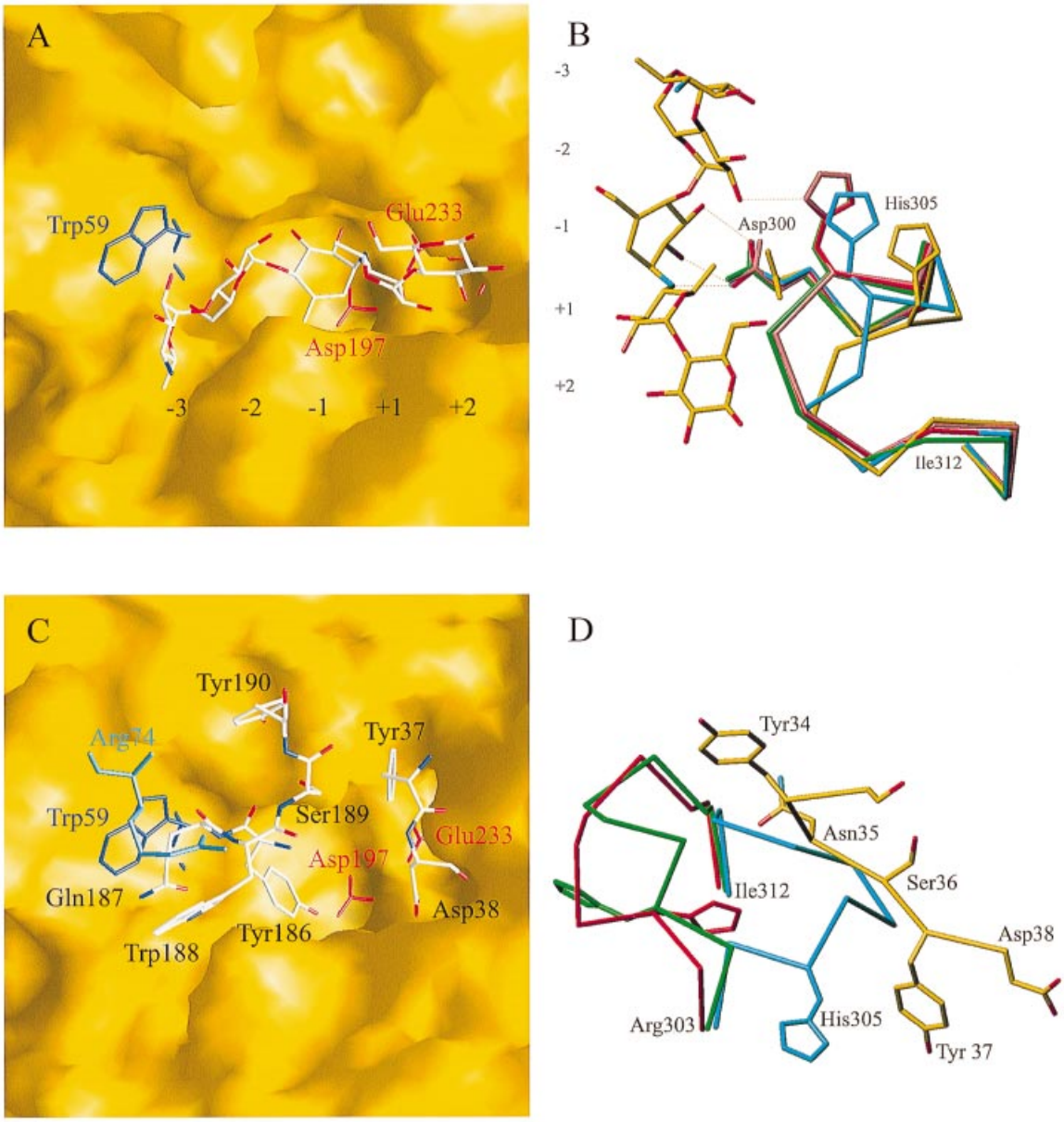

Figure 2 A close-up of the active site of HPA

(**A**) A model of the complex formed between HPA and a trestatin-derived inhibitor (produced using GRASP [33]). The five occupied subsites are labelled −3 to +2 [32]. The catalytic residues, nucleophile and acid/base catalyst are all shown in red. (**B**) Structure of the trestatin-derived inhibitor bound at the active site of HPA. The superimposed α-carbon backbone traces obtained in the region of the flexible loop with free HPA (blue) [3], free PPA (yellow) [4], acarbose-complexed PPA (pink) [20], acarbose- and B4-complexed HPA (red and green respectively) are also shown. The side chain of His-305 and Asp-300 are shown with the five structures. (**C**) The same as (**A**), but with selected residues of the proteinaceous inhibitor interacting in the active site. The inhibitor residue Arg-74 lying in front of the hydrophobic gate composed by the enzyme residue Trp-59 (dark blue) and inhibitor residues Gln-187 and Trp-188 (atom type) is shown in a lighter shade of blue. (**D**) The same loop region as in (**B**), in the α-AI–HPA1 (red) and α-AI–HPA2 (green) complexes, with selected neighbouring inhibitor residues (atom type); the loop in free HPA (blue) is also shown.

contains opposite orientations of the carbonyl main-chain groups at residues 237 and 239 between the free and complexed structures of HPA. This loop constitutes the surface edge at the reducing-end periphery of the active-site depression. Residues from this loop and from the 'flexible loop' discussed above are involved in the architecture of subsite +2. Machius et al. [26] have reported that Leu-237 participates in binding substrate at subsite +3 in PPA. No sugar unit bound at this external subsite was observed in the present structures; however, the movements observed around residues 237–240 in the acarbose- and B4-complexed HPA suggest that some interaction occurred with the inhibitor molecules, inducing the loop changes.

α-AI binding to HPA

Two crystal forms of the complex between HPA and α-AI, obtained at different pH values, have been used in order to

Table 2 Hydrogen bonds between HPA and inhibitors in the active site (a) and in neighbouring regions (b)

*Only present in α-AI–HPA1; †only present in α-AI–HPA2; ‡not present in the PPA–α-AI structure.

(a)

	Active site			
	HPA–acarbose and HPA–B4 complexes		α-AI–HPA1 and α-AI–HPA2 complexes	
Subsite	Sugar atom	HPA atom	α-AI atom	HPA atom
−3	O-4	Thr-163 O	Trp-188 NE1	Thr-163 OG1‡
	O-5	Gln-63 NE2		
−2	O-2	His-305 ND1		
	O-6	Trp-59 O		
	O-6	Gln-63 NE2		
−1	O-2	Arg-195 NH2		
	O-2 and O-3	His-299 NE2	Tyr-186 OH	His-101 NE2
	O-2	Asp-300 OD2	Tyr-186 OH	Asp-197 OD2
	O-3	Asp-300 OD1		
	O-6	His-101 NE2		
	O-6	Asp-197 OD2		
+1	O-2	His-201 NE2	Asp-38 OD1 and OD2	His-201 NE2
	O-3	Glu-233 OE1	Tyr-37 OH	Glu-233 OE2
	N-4	Glu-233 OE2	Tyr-37 OH	Asn-298 ND2
	N-4	Asp-300 OD2	Ser-189 OG	Asp-300 OD1 and OD2
			Tyr-190 OH	Asp300 O and OD2
+2	O-2 and O-3	Lys-200 NZ	Asp-38 O	Lys200 NZ
	O-6	Gly-306 O	Asp-38 OD1	Tyr151 OH
			Met-40 N	Glu240 OE2

(b)

Extended protein–protein interactions (· · · ·) in complexes α-AI–HPA1 and α-AI–HPA2

α-AI atom–HPA atom	α-AI atom–HPA atom	α-AI atom–HPA atom
Lys-13 NZ · · · · Asn-270 OD1*‡	Asn-35 OD1 · · · · Ser-311 N	Asn-35 OD1 · · · · Ile-312 N*‡
Asn-35 ND2 · · · · Ser-311 OG	His-73 O · · · · Asp-356 OD2‡	Arg-74 O · · · · Asn-352 ND2†‡
Gln-75 O · · · · Gln-349 NE2*‡	Ser-78 N · · · · Glu-149 O	Ser-78 O · · · · Glu-149 O‡
Arg-108 NH2 · · · · Glu-149 OE2†‡	Asn-115 OD1 · · · · Asn-150 ND2‡	

analyse the interaction of the human enzyme with the proteinaceous inhibitor.

In both structures, elements of the inhibitor establish a network of hydrogen bonds with the residues of the substrate-docking region. Figures 2(A) and 2(C) and Table 2 show that interactions occurring in the region of subsites −1, +1 and +2 are highly conserved in the patterns of inhibition by various compounds. The hydrophobic interactions occurring between the substrate's surface and the hydrophobic residues lining the entrance of the cleft (subsite −2, −3) involve a cluster of inhibitor residues being stacked against enzyme residues (see Figure 2C). These interactions are corroborated by protein–protein interactions involving areas further away from the catalytic centre, namely the 'flexible loop' (residues 303–312), the loops comprising residues 237–240 and 347–354, and the loop formed by residues 140–150 from domain B. It is tempting to speculate that these regions may correspond to areas of interaction with the polymeric substrate, amylose.

A comparison of the HPA–α-AI and the PPA–α-AI complexes shows additional hydrogen bonds between the inhibitor and domain B of the human enzyme. Both the pig and human enzymes have different amino acid sequences in this region, raising the possibility that subtle differences exist in substrate specificities between the two enzymes.

A different network of interactions is also observed in the loop regions 303–312 and 347–357 of domain A (Table 2). These regions of this domain undergo pH-sensitive structural changes upon inhibitor binding, suggesting that the contact with these regions might be produced in alternative ways (see Figure 2D).

Inhibitor residue Arg-74

The long loop at residue positions 347–354, which protrudes into the solvent in the free HPA structure, interacts with the region corresponding to residues 73–75 of the inhibitor close to the processing site (Asn-77) required for the activation of the inhibitor. Protein engineering studies [27] suggested that residue Arg-74 was a critical part of a triad of residues (Trp-188, Arg-74 and Tyr-190), which closely matches the tripeptide sequence that forms the inhibitory region in the PPA inhibitor, Tendamistat [28]. In our previous structure of the PPA–α-AI complex, this segment of the inhibitor was not well defined in the electron-density map, and the side chain of Arg-74 was not seen. The present structures, and particularly that obtained at the higher pH value, made it possible to assess the features of this important segment of the inhibitor and its environment in interaction with HPA. A well-defined patch of electron density was observed corresponding to the side chain of Arg-74. This residue protrudes at the enzyme/inhibitor interface, lying in front of the hydrophobic gate formed at the entrance of the active-site cleft by the inhibitor residues Gln-187 and Trp-188, which stack against

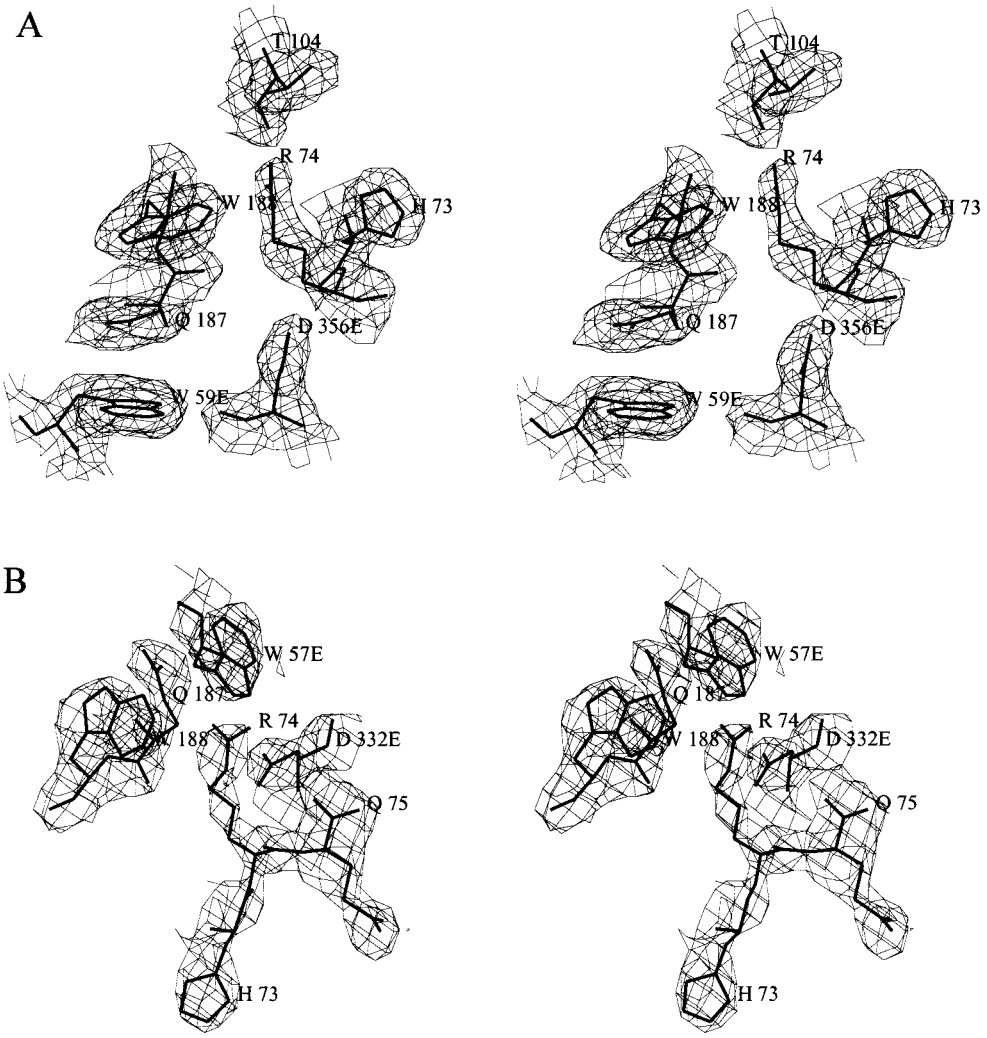

Figure 3 Hydrophobic stacking features at the entrance of the active site

A stereoview of the electron-density map (2 $F_{obs} - F_{calc}$)exp(iα_{calc}) (1σ level). The inhibitor residue Arg-74 is shown from the α-AI–HPA2 complex in the present study (**A**), and the complex between α-AI and the α-amylase from *Tenebrio molitor* (TMA) (**B**) [29]. The residue numbers of HPA and TMA are denoted by an 'E' suffix.

residue Trp-59 of the enzyme (Figure 3A). This stacking interaction is reminiscent of that produced in the PPA–Tendamistat complex by a segment containing the staggered side chains of the triplet Trp-18 (stacking against $Trp\text{-}59_E$; see the legend to Figure 3 for further explanation)/Arg-19/Tyr-20. However, in the latter structure, the inhibitor segment binds directly to the catalytic site, whereas in the HPA–α-AI structures this feature is rotated outwards, towards the solvent. Consequently, Arg-74 of α-AI does not have the same role as Arg-19 of Tendamistat, i.e. a direct interaction with a catalytic residue. Instead, Arg-74 interacts with another inhibitor residue, Thr-104 (Figure 3A). In the structure of the α-amylase from *Tenebrio molitor* (designated as TMA in the legend to Figure 3) in complex with α-AI [29], the inhibitor segment from residues 73–76 also showed a well-defined patch of electron density, and a clear-cut electron density corresponded to the side chain of Arg-74 (see Figure 3B). However, the orientation of the Arg-74 side chain was twisted by about 180 ° compared with that observed in the α-AI–HPA structure shown in Figure 3(A), and therefore it switched its interaction from the inhibitor residue Thr-104 to the neighbouring enzyme residue, Asp-332 (Asp-356 in the present structures). Taken together, our structural analyses show that the side chain of residue Arg-74 is able to adopt different orientations sweeping in front of the stacking feature ($Trp\text{-}59_E$, $Gln\text{-}187_I$ and $Trp\text{-}188_I$) from the inhibitor surface to the enzyme surface.

Conformational changes in the HPA–α-AI structures

The 'flexible loop' (residues 303–312) that is involved in the architecture of subsites −2 and +2 adopts various conformations, according to the structure of the ligand. While this loop moves 'in' towards the saccharide ligand, it moves 'out' towards the solvent in the complex with the proteinaceous inhibitor. In addition, the 'flexible loop' conformation appears to be pH-sensitive, as we identified two different conformations in the crystal forms grown at pH 6.3 and 7.8. The different conformations observed in this area of the human enzyme molecule in interaction with the bean inhibitor are shown in Figure 2(D). The

maximum main-chain movement is 5.9 Å at Gly-306. The side chain of residue His-305, which is specific for mammalian α-amylases and which forms a strong hydrogen bond with the sugar ring bound at subsite -2 of the active site, is rotated by about 150 ° in the crystal structure at the higher pH. In this latter structure, His-305 loses its hydrogen bond with the carbonyl main-chain atom of the inhibitor residue Tyr-34 and, as a result, rotates towards the solvent.

As noted above, the conformation of the catalytic residue Asp-300 is identical both in free HPA and in HPA complexed with carbohydrates (Figure 2B). In contrast, in the two structures of HPA in complex with the *P. vulgaris* α-AI, the side chain of Asp-300 adopts a clearly different position, indicating that, in the human enzyme, this residue is able to undergo conformational changes.

In conclusion, the active site of human α-amylase has been investigated using two carbohydrate inhibitors and a proteinaceous inhibitor. The structural analysis of the network of interactions provides insight into the mechanistic role of the various important residues of the human enzyme, and sheds light on the predominant binding mode of the trestatin-derived inhibitors. Carbohydrate in the form of starch represents the majority of the human diet. Cleavage of starch by α-amylases constitutes the first step of the process, and high affinity/selectivity α-amylase inhibitors have potential applications in various fields, from the treatment of diabetes to crop protection. Detailed knowledge of the inhibition of α-amylase by various inhibitors is a necessary prerequisite to any structure-based rational design of specific α-amylase synthetic inhibitors.

This work was funded by CNRS and Bayer Pharma. We thank Dr B. Oberkampf, Dr J. C. Crave and Dr H. Bischoff (Bayer Pharma) for their helpful support.

REFERENCES

1 Henrissat, B. (1991) Biochem. J. **280**, 309–316
2 Coutinho, P. M. and Henrissat, B. (1999) in Recent Advances in Carbohydrate Bioengineering (Gilbert, H. J., Davies, G. J., Henrissat, B. and Svensson, B., eds.), pp. 3–12, The Royal Society, Cambridge, in the press
3 Brayer, G. D., Luo, Y. and Withers, S. G. (1995) Protein Sci. **4**, 1730–1742
4 Qian, M., Haser, R. and Payan, F. (1993) J. Mol. Biol. **231**, 785–799
5 Rydberg, E. H., Sidhu, G., Vo, H. C., Hewitt, J., Cote, H. C., Wang, Y., Numao, S., MacGillivray, R. T., Overall, C. M., Brayer, G. D. and Withers, S. G. (1999) Protein Sci. **8**, 635–643
6 Ferey-Roux, G., Perrier, J., Forest, E., Marchis-Mouren, G., Puigserver, A. and Santimone, M. (1998) Biochim. Biophys. Acta **1388**, 10–20
7 Le-Berre-Anton, V., Bompard-Gilles, C., Payan, F. and Rougé, P. (1997) Biochim. Biophys. Acta **1343**, 31–40
8 McPherson, A. (1982) Preparation and Analysis of Protein Crystals, pp. 82–127, John Wiley, New York
9 Weber, P. C. (1991) Adv. Protein Chem. **24**, 409–411
10 Otwinowski, Z. and Minor, W. (1997) Methods Enzymol. **276**, 307–327
11 Navaza, J. (1994) Acta Crystallogr. **A50**, 157–163
12 Bompard-Gilles, C., Rousseau, P., Rougé, P. and Payan, F. (1996) Structure **4**, 1441–1452
13 Castellano, E. E., Oliva, O. and Navaza, J. (1992) J. Appl. Crystallogr. **25**, 281–284
14 Matthews, B. W. (1968) J. Mol. Biol **33**, 491–497
15 Brünger, A. T., Kuriyan, J. and Karplus, M. (1987) Science **35**, 458–460
16 Brünger, A. T. (1996) X-PLOR Version 3.843 Manual, Yale University Press, New Haven
17 Read, R. J. (1986) Acta Crystallogr. **A42**, 140–149
18 Brünger, A. T. (1992) Nature (London) **355**, 472–475
19 Laskowski, R. A., MacArthur, M. W., Moss, D. S. and Thornton, J. M. (1993) J. Appl. Crystallogr. **26**, 283–291
20 Qian, M., Buisson, G., Duée, E., Haser, R. and Payan, F. (1994) Biochemistry **33**, 6284–6294
21 Gilles, C., Astier, J. P., Marchis-Mouren, G., Cambillau, C. and Payan, F. (1996) Eur. J. Biochem. **238**, 561–569
22 Strokopytov, B., Knegtel, R. M., Penninga, D., Rozeboom, H. J., Kalk, K. H., Dijkhuizen, L. and Dijkstra, B. W. (1996) Biochemistry **35**, 4241–4249
23 Brzozowski, A. M. and Davies, G. J. (1997) Biochemistry **36**, 10837–10845
24 Dauter, Z., Dauter, M., Brzozowski, A. M., Christensen, S., Borchert, T. V., Beier, L., Wilson, K. S. and Davies, G. J. (1999) Biochemistry **38**, 8385–8392
25 Larson, S. B., Greenwood, A., Cascio, D., Day, J. and McPherson, A. (1994) J. Mol. Biol. **235**, 1560–1584
26 Machius, M., Vertesy, L., Huber, R. and Wiegand, G. (1996) J. Mol. Biol. **260**, 409–421
27 Mirkov, T. E., Evans, S. V., Wahlstrom, J., Gomez, L., Young, N. M. and Chrispeels, M. J. (1995) Glycobiology **5**, 45–50
28 Wiegand, G., Epp, O. and Huber, R. (1995) J. Mol. Biol. **247**, 99–110
29 Nahoum, V., Farisei, F., Le-Berre-Anton, V., Egloff, M. P., Rougé, P., Poerio, E. and Payan, F. (1999) Acta Crystallogr. **D55**, 360–362
30 Luzzati, P. V. (1952) Acta Crystallogr. **5**, 802–810
31 Schmidt, D. D., Frommer, B., Junge, L., Müller, W., Wingender, W. and Trusheit, E. (1977) Naturwissenschaften **64**, 535–536
32 Davies, G. J., Wilson, K. S. and Henrissat, B. (1997) Biochem. J. **321**, 557–559
33 Nicholls, A. J. (1993) GRASP Manual. Graphical Representation and Analysis of Surface Properties, Columbia University, New York

Received 2 September 1999/9 November 1999; accepted 25 November 1999